Radiocarbon, Vol 56, Nr 3, 2014, p 1151–1166 DOI: 10.2458/56.16505

RADIOCARBON DATING OF LATE PLEISTOCENE MARINE SHELLS FROM THE SOUTHERN NORTH SEA

F S Busschers[1,2] • F P Wesselingh[3] • R H Kars[4] • M Versluijs-Helder[5] • J Wallinga[4,6] • J H A Bosch[1] • J Timmner[7] • K G J Nierop[8] • T Meijer[3,9] • F P M Bunnik[1] • H De Wolf[9]

ABSTRACT. This article presents a set of Late Pleistocene marine mollusk radiocarbon (AMS) age estimates of 30–50 ^{14}C kyr BP, whereas a MIS5 age (>75 ka) is indicated by quartz and feldspar OSL dating, biostratigraphy, U-Th dating, and age-depth relationships with sea level. These results indicate that the ^{14}C dates represent minimum ages. The age discrepancy suggests that the shells are contaminated by younger carbon following shell death. The enigmatic ^{14}C dates cannot be "solved" by removing part of the shell by stepwise dissolution. SEM analysis of the Late Pleistocene shells within a context of geologically younger (recent/modern, Holocene) and older (Pliocene) shells shows the presence of considerable amounts of an intracrystalline secondary carbonate precipitate. The presence of this precipitate is not visible using XRD since it is of the same (aragonitic) polymorph as the original shell carbonate. The combination of nanospherulitic-shaped carbonate crystals, typical cavities, and the presence of fatty acids leads to the conclusion that the secondary carbonate, and hence the addition of younger carbon, has a bacterial origin. As shell material was studied, this study recommends an assessment of possible bacterial imprints in other materials like bone collagen as well.

INTRODUCTION

The effect of contamination by admixing of younger carbon becomes more acute with increasing age (Aitken 1990; van der Plicht 2012). Admixture of only 1% of modern carbon reduces the radiocarbon age of a 40-kyr sample by ~17%, an effect that becomes larger with older samples. Contamination especially affects accelerator mass spectrometry (AMS) ^{14}C-dated material since this relies on very small sample quantities. Contamination effects and the resulting apparent young ages have been described for marine shells (Mangerud 1972; Nadeau et al. 2001). Carbonate diagenesis is generally regarded as the cause for incorporation of younger ^{14}C into the crystal structure (Mangerud 1972; Goslar and Pazdur 1985; Aitken 1990; Nadeau et al. 2001; Magnani et al. 2007; Webb et al. 2007; Douka et al. 2010; Price et al. 2011).

We observed similar young aging effects on shells from three cores near Wassenaar, Amsterdam, and Amersfoort in the western Netherlands (Figure 1). The sedimentary record of these cores consists of fluvial (Rhine and Meuse) and/or estuarine late Pleistocene strata that locally contain high concentrations of marine shells (Busschers et al. 2007; Appendix 1, cores B30F0490, B25E0913 and B32B0119). ^{14}C dating on some of these marine shells showed strikingly young ages (up to 39 ^{14}C kyr BP; Table S1) compared to quartz optical stimulated luminescence (OSL), uranium-thorium (U-Th) dating, and pollen biostratigraphy (Appendix 1). These latter age constraints point to an age older than 60 kyr, indicating the ^{14}C ages could reflect minimum ages. No more shell material was available from these cores to perform further analysis.

In order to elucidate causes for the very young ^{14}C ages and test whether carbonate diagenesis could also explain the observed age discrepancies, two new cores were drilled (Figure 1). One core was aimed to penetrate Eemian marine sediments in the northern part of the Netherlands, while the other one was aimed for much older (Pliocene) marine sediments in the south, meaning that ^{14}C ages should result in instrumental background ages. Besides new ^{14}C AMS analyses on the marine

1. TNO - Geological Survey of the Netherlands, Utrecht, the Netherlands.
2. Corresponding author. Email: freek.busschers@tno.nl.
3. Naturalis Biodiversity Center, Leiden, the Netherlands.
4. Centre for Luminescence Dating, Delft University of Technology, Faculty of Applied Sciences, Delft, the Netherlands.
5. Department of Inorganic Chemistry and Catalysis, Utrecht University, Utrecht, the Netherlands.
6. Soil Geography and Landscape Group, Wageningen University, Wageningen, the Netherlands.
7. TNO - Applied Environmental Chemistry, Utrecht, the Netherlands.
8. Department of Earth Sciences - Geochemistry, Utrecht University, Utrecht, the Netherlands.
9. WMC Kwartair Consultants, Alkmaar, the Netherlands.

shell material, we also performed quartz and feldspar pIR-IR 290 OSL dating and biostratigraphical analysis (pollen, diatoms, and mollusk species) in order to place the dated material into a firm chronostratigraphical context. This new core material made it possible to extensively study possible post-mortem changes in chemical composition and carbonate crystal structure.

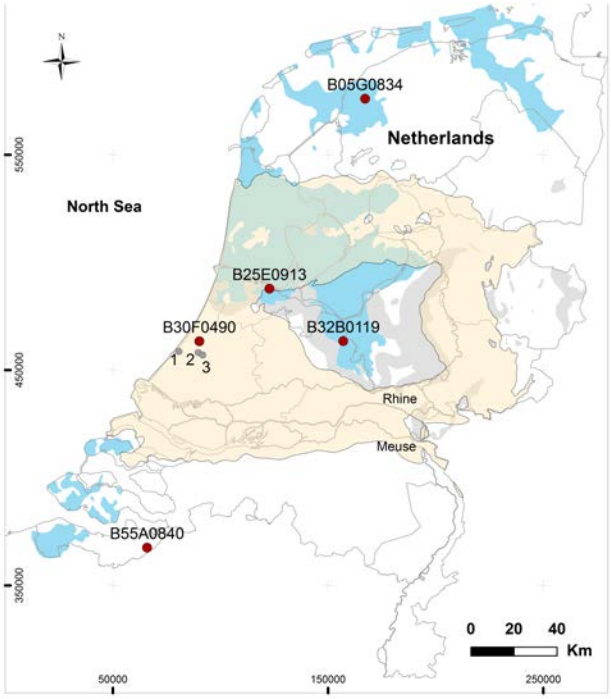

Figure 1 Core locations depicted within the context of preserved MIS5 age sediments (blue), MIS4-2 age Rhine-Meuse record (yellow transparent), and MIS6 age glacio-tectonic ridges (gray) (Busschers et al. 2007). Main cores containing MIS5 age and/or Pliocene shells are indicated in red. Cores with Holocene shells are indicated in gray (for numbers see Table S1).

This article first presents results of a multidisciplinary comparison between ^{14}C dating and other dating techniques in the two new boreholes. We show that the ^{14}C-dated material from these boreholes has a true geological age older than ~75 ka (MIS5) and that the ^{14}C ages therefore must represent only minimum ages. Then, we analyze the nature of possible contaminant mechanisms in order to elucidate causes for the very young ^{14}C ages.

GEOLOGICAL, BIOSTRATIGRAPHICAL, AND CHRONOLOGICAL CONTEXT OF SHELL MATERIAL

Our primary research core is located near the town of Sneek (B05G0834; Figure 1) in the northern Netherlands. The area was covered by the Fennoscandian ice sheet during the late Saalian (MIS6) as indicated by a 2-m-thick till (21.55–19.37 m; Unit DR; Figure 2). Above the till, a distinct interval of medium-grained sand with mm to cm thick mud drapes is present (19.37–10.35 m; Unit EE). The repetitive clay draping suggests deposition under tidal (estuarine) conditions. At some levels, the distinct layering is disturbed by bioturbation. At the base of the interval, some reworked peat pebbles are present. The upper part of the estuarine sequence (11.45–10.35 m) is disturbed by periglacial activity. Sharply overlying the estuarine interval is a thin layer of medium-grained, well-sorted sands of eolian origin (10.35–9.55 m; Unit BX). The succession is covered by estuarine sediments of Holocene age (9.55–0 m; Unit NA).

Concentrations of shells occur in several levels throughout estuarine Unit EE (Figure 2) with characteristic species being *Peringia ulvae*, *Cerastoderma edule*, *Macoma balthica*, *Mytilus edulis*, *Spisula subtruncata*, and *Venerupis senescens* (Appendix 4; Meijer 2008). The association points to

shallow marine high mesohaline conditions for the lower part of the unit and open marine polyhaline conditions for its upper part. In the North Sea area, the species *Venerupis senescens*, *Nassarius pygmaeus*, *Haminea navicula*, *Gastrana fragilis*, *Lucinella divaricata*, *Acanthocardia paucicostata*, *Parvicardium exiguum*, and *Tellina distorta*, found in this interval, are only known from the Eemian (MIS5e, ~120 ka: Meijer and Preece 1995; Meijer 2008). Diatom analysis of several shell-bearing levels in Unit EE yield similar environmental interpretations (TNO-Deltares, unpublished, 2010; Appendix 5). The lower part of the interval contains a species assemblage, dominated by *Cymatosira belgica*, that points to vegetated, shallow marine, low-energetic conditions. Upwards, a gradual transition towards higher energy conditions occurs, as shown by the occurrence of species like *Biddulhia rhombus* and *Melosira sulcata* and the more sandy character of the sediments.

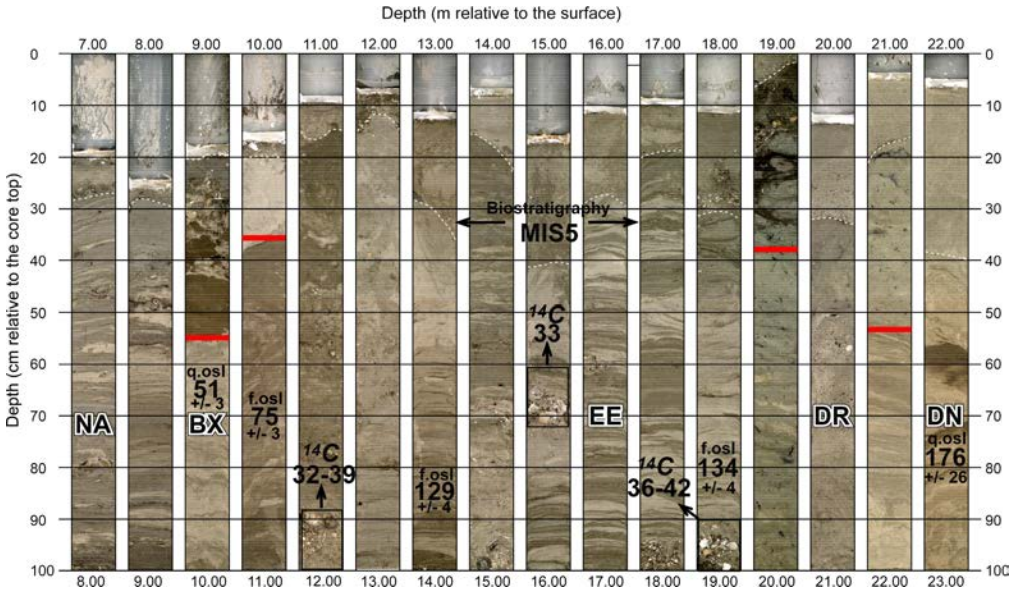

Figure 2 Core photographs, sedimentary units (Westerhoff et al. 2003; Busschers et al. 2007) and age constraints of core B05G0834. ^{14}C ages: ^{14}C kyr BP age range (Table S1). OSL: q.osl = quartz age; f.osl = feldspar age. Red lines are boundaries between sedimentary units. Depths are reported in meters below sea level (Dutch Ordnance Level: NAP).

From the clayey intervals of the core, detailed palynological records were obtained (Appendix 6: Bunnik 2008). The pollen assemblages fully resemble stages of warm, interglacial vegetation successions known from the Eemian type sites Amersfoort and Amsterdam Terminal (Zagwijn 1961, 1996; Cleveringa et al. 2000; Van Leeuwen et al. 2000) whereby the lower part of the sequence (19.34–19.20 m) correlates to pollen zone E4 and the upper part (16.66–10.34 m) to pollen zone E5 and possibly the transition into E6 (Bunnik 2008).

From core B05G0834, five samples were collected for quartz and pIR-IR 290 feldspar OSL dating. Three samples were taken from the shell-bearing unit (Unit EE) and two from underlying and overlying units (DN and BX, respectively, Figure 2). An extensive description of the sampling technique and the applied quartz and pIR-IR 290 feldspar OSL protocols is provided in Appendix 3.

Quartz OSL ages from the shell-bearing unit EE give an age range of 87–165 OSL kyr (late MIS6 and MIS5). Quartz OSL ages from underlying and overlying units are clearly older (176 OSL kyr) and younger (51 OSL kyr), respectively (Figure 2; Appendix 3_3). Feldspar pIR-IR 290 ages are in general agreement with the quartz OSL ages. The age range of 75–134 OSL kyr obtained from

the samples in shell-bearing unit EE (Appendix 3_4) also suggest a MIS5 age, which is largely in agreement with the biostratigraphical age constraints. Alike for the quartz results, Feldspar pIR-IR 290 ages from underlying and overlying units are also clearly older (255 OSL kyr) and younger (59 OSL kyr), respectively (Figure 2; Appendix 3_5). A best-estimate age list for the B05G0834 core that contains quartz OSL ages and post IR-IR ages is depicted in Appendix 3_5.

We also investigated a second core from the southern Netherlands (B55A0840, Figure 1). The core contains a sequence of glauconite-rich sands that characterize Neogene deposits in the area (Appendix 1). Both the core lithology as well as the occurrence of *Astarte incerta* (an indicator for a Pliocene age, Moerdijk et al. 2010) shows the sediments are part of the Pliocene Oosterhout Formation (Westerhoff et al. 2003). Besides *A. incerta*, the unit is also characterized by concentrations of *Arctica islandica* (Appendix 1, Unit OO, >6.70 m). The sediments are covered by Weichselian and Holocene sediments (Unit BX and NA).

RADIOCARBON DATING

Material

From the shell-bearing levels of core B05G0834 (Unit EE, Figure 2), seven shell samples were collected for ^{14}C dating (Table S1). At a depth of ~12 m below the surface (bs), three shell samples were collected of the species *Venerupis senescens*, *Macoma balthica*, and *Cerastoderma edule*. At a depth of ~15.7 mbs, one sample of *Ostrea edulis* was collected. At a depth of ~19 mbs, three shell samples were collected of *V. senescens*, *M. balthica*, and *C. glaucum*. The selected shells were intact and showed a well-preserved periostracum. The shells must have remained below groundwater level after deposition, inhibiting the loss of organic matter through oxidation. Reworking of the shells has been minimal.

From this same core, at ~12 mbs, we additionally collected two bulk samples of *C. edule* fragments (Table S1) in order to date the intracrystalline shell structure. The selected fragments also retained a well-preserved periostracum.

From the shell-bearing levels of core B55A0840 (Unit OO), two shell samples of species *A. incerta* and *A. islandica* were collected for ^{14}C dating (Table S1). The selected shells were intact and showed a well-preserved periostracum.

Protocols

^{14}C AMS dating of shells from cores B05G0834 and B55A0840 was performed at the Department of Nuclear Engineering and Management, University of Tokyo (Japan; lab code MTC). The shells were inspected under a magnifier and physically cleaned using a dental drill to remove interstitial structures other than walls. The samples were cleaned with distilled water in an ultrasonic bath. They were then dried in an oven (~40–60°C) and weighed.

Sample sizes of 200–300 mg were used for stepwise selective dissolution of the shells. Our graphitization procedure consisted of three steps (Yokoyama et al. 2007). The first involves CO_2 production followed by CO_2 purification. Then, the gas was reduced in the graphitization reactor with Fe catalyst (250-mesh grain size) under a hydrogen atmosphere. All the carbonate samples were dissolved in phosphoric acid in a vacuum test tube (Vacutainer®). Samples were placed in the tube and evacuated using a needle attached to the vacuum line system. The tube was then placed in the heat block (60°C) with phosphoric acid introduced through an air-tight cylinder. The tube was removed from the heat block when the sample dissolution was complete. The product CO_2 was then passed through the vacuum line and cryogenically transferred into the graphitization reactor via a series of

cryogenic traps to purify the gas. Graphite forms on the surface of the prereduced Fe powder in a hydrogen atmosphere heated to about 630°C. The graphite was then pressed into a into target holders and analyzed using AMS (Matsuzaki et al. 2004). Instrumental background levels, monitored using the international marble standard IAEA C1 (Rozanski et al. 1992), were 0.19–0.39 $F^{14}C$.

AMS ^{14}C dating of the intracrystalline fraction from the two bulk subsamples of *C. edule* shells from core B05G0834 was performed at the Centre for Isotope Research (CIO) of the University of Groningen (the Netherlands; lab code GrA). The subsamples were placed in 1M HCl until the noncarbonate intracrystalline fraction (0.29 and 0.35%) remained. After pretreatment, the organic AMS samples were combusted in an automated Carlo Erba (type NC2500) elemental analyzer (EA). The evolved CO_2 was cryogenically trapped and transferred to the graphitization setup. Graphitization was performed using the method of reduction under hydrogen excess with iron powder as catalyst. The graphite was then pressed into a into target holders and analyzed using AMS (Aerts-Bijma et al. 1997, 2001; van der Plicht et al. 2000). Instrumental background ^{14}C levels, monitored using the Groningen Standaard 35 carbonate, were 0.26 $F^{14}C$.

RESULTS

In core B05G0834, ^{14}C ages of the individual shells vary between 32–42 ^{14}C kyr BP (Table S1; MTC-12236-45). Both at the ~12 and ~19 mbs levels, we observed that ages from *C. edule* were youngest while ages from *V. senescens* were oldest. For all species that were dated at these different levels, we observed an increase in age (~2–3 ^{14}C kyr; Table S1). From the same core, the two noncarbonate bulk samples of *C. edule* from ~12 mbs gave ages of 30–33 ^{14}C kyr BP (Table S1; GrA 53002-3).

For the upper shell level of core B05G0534 (Table S1; MTC 12236-45), the ^{14}C ages with different dissolution values are plotted in Figure 3. Marked pattern variations occur within individual shells. Overall ^{14}C ranges remain, however, within ~5 kyr. The ages from the *M. balthica* lack a systematic trend with increasing dissolution values and vary between 35 and 37 ^{14}C kyr BP (Figure 3). The ^{14}C ages from the *C. edule* decrease with higher dissolution values from 36 ^{14}C kyr BP (0–10% dissolution) to about 32 ^{14}C kyr BP (dissolution 83–100%) (Figure 3). *Venerupis senescens* ages increase with higher dissolution values (Figure 3) from 35.5 ^{14}C kyr BP (0–10% dissolution) to ~40 ^{14}C kyr BP (dissolution 83–100%). For core B55A0840, both dates gave background ages >50 ^{14}C kyr BP (Table S1; MTC 15005-6).

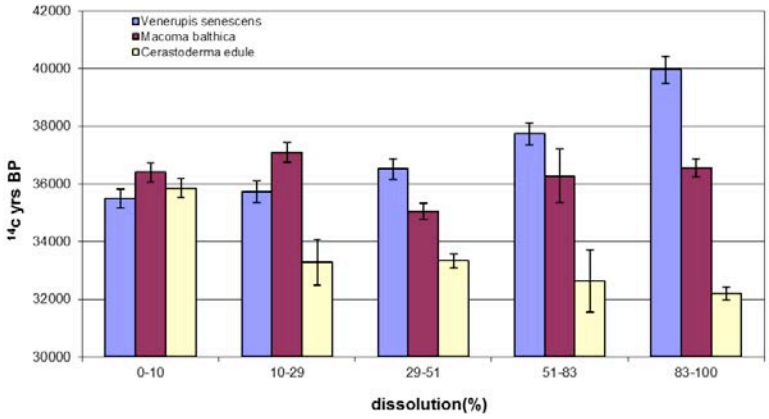

Figure 3 ^{14}C dating results using stepwise dissolution of Late Pleistocene *Macoma balthica*, *Cerastoderma edule*, and *Venerupis senescens* from core B05G0834.

SHELL STRUCTURE AND DIAGENESIS

Material

From core B05G0834, three aragonitic (*M. balthica*, *C. edule*, and *V. senescens*) and a calcitic (*O. edulis*) species were selected for investigation of the shell structure in order to assess possible diagenetic alterations. From core B55A0840, two aragonitic shell samples were selected (*A. incerta*, *A. islandica*). The samples from cores B05G0834 and B55A0840 will be henceforth referred to as the Late Pleistocene shells and Pliocene shells, respectively (Table S1).

In order to compare diagenesis of these fossil shells, we selected shell samples from Holocene sediment and modern beach settings that should represent unaltered conditions (Table S1). A set of Holocene shells was used for which the corresponding shells have previously been used for dating Holocene coastal (back) barrier formation (TNO-Deltares, unpublished, 2010; Hijma et al. 2009). These samples are henceforth referred to as the Holocene mollusks. Dating of these shells was performed at the Van de Graaff Laboratory of Utrecht University (the Netherlands; lab code UtC) using the protocol described in Appendix 1 for core B30F0490. The results gave ^{14}C ages between 4.5 and 6.0 ^{14}C kyr BP (TNO-Deltares, unpublished, 2010; Hijma et al. 2009). Furthermore, three fresh-looking aragonitic species (including *Venerupis senegalensis*, a close relative of the extinct *V. senescens*) and one calcitic shell (*O. edulis*) collected from the beach at Noordwijk several decades ago, were investigated: these are further indicated as "modern shells."

From all selected samples, the outer 20% was removed using a Scheibler system. To allow multiple types of analyses on the same shell, each shell was divided into a number of fragments. The fragments were used for scanning electron microscopy (SEM) in combination with X-ray microanalysis (XRMA), X-ray powder diffraction (XRD), $\delta^{13}C/\delta^{18}O$ isotope analysis, and pyrolysis-gas chromatography-mass spectrometry, which all are used to investigate possible diagenesis. The applied methods are described in Appendix 2.

RESULTS

SEM, XRMA, and XRD

This section describes the analysis results of the modern and Late Pleistocene *M. balthica* (aragonitic) and *O. edulis* (calcitic) shells in detail. The description of these shells is representative for the features observed in the other shells (Table S1). SEM results of the modern, Holocene, Late Pleistocene, and Pliocene shells are available in Appendix 7. XRMA results (available for the modern and Late Pleistocene shells only) and XRD data are available in Appendices 8 and 9, respectively.

Modern Shells

SEM photographs of the modern (aragonitic) *M. balthica* are depicted in Figures 4A,B and Appendix 7. The modern *M. balthica* shows a relative porous structure of 50–200 nm sized crystals separated by intracrystalline zones. Some of the crystals have a nanospherulitic shape. Larger crystals were not observed, although this might be related to the orientation of the cross-sectional surface. The dominance of C, O, and Ca, and the heterogenic spatial distribution of these elements in the XRMA data (Appendix 8), suggests all crystals are composed of carbonate. The presence of peaks at 30.6°, 38.7°, and 53.9° in the XRD data indicate the carbonate polymorphic form is aragonitic (Appendix 9). The absence of a peak at 34.3° shows there is no calcite present. Other modern aragonitic shells showed some calcite to be present in the matrix (Table S1; Appendix 9).

SEM photographs of a modern (calcitic) *O. edulis* are given in Figure 4G. The shell shows a highly porous internal structure with typical 1–10 µm sized crystals. XRD of the modern *Ostrea edulis*

shows a typical calcitic carbonate composition with a major peak at 34.3° (Appendix 9). The analysis shows no evidence for the presence of aragonite (Table S1).

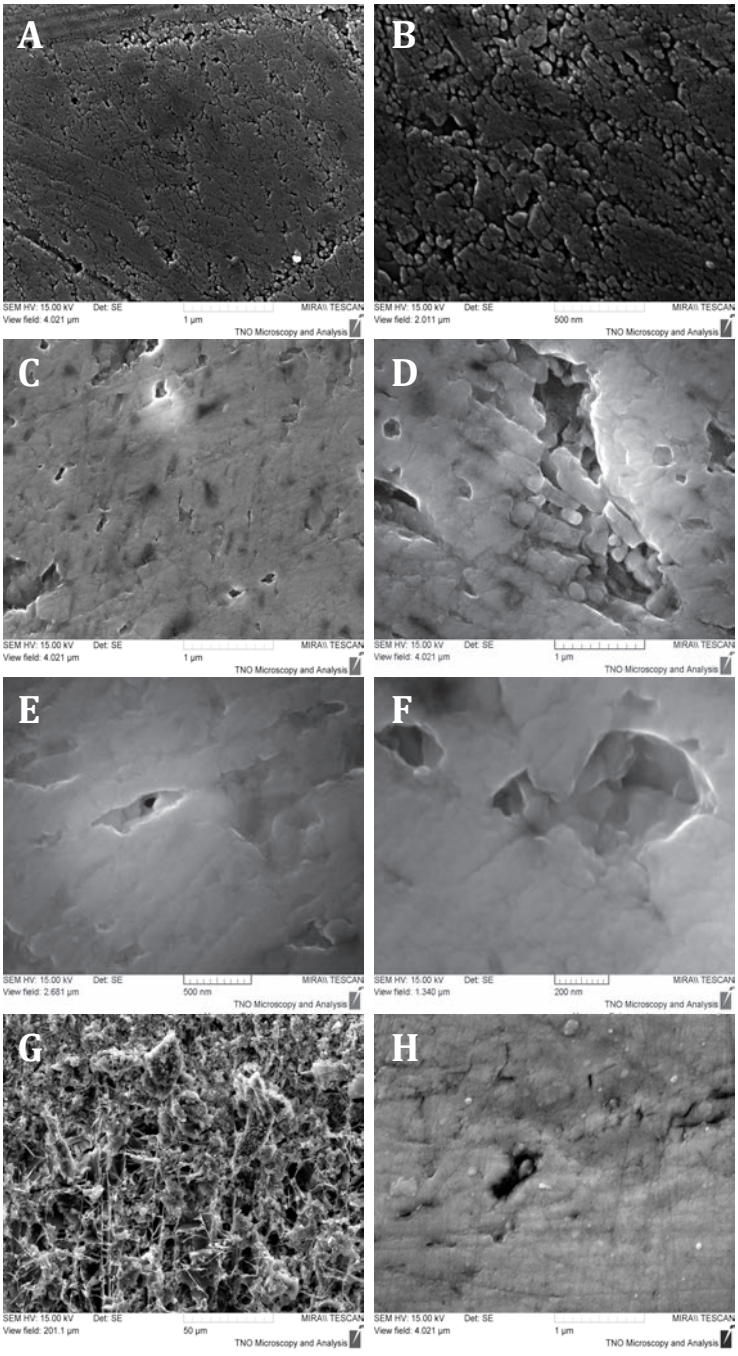

Figure 4 SEM photographs of a modern *Macoma balthica* (A, B), Late Pleistocene *Macoma balthica* (C, D, E, F), modern *Ostrea edulis* (G), and Late Pleistocene *Ostrea edulis* (H). All photographs were focused on representative features observed in the specific mollusks. This data and all other SEM data are available in Appendix 7.

Late Pleistocene Shells

SEM photographs of the Late Pleistocene *M. balthica* are depicted in Figures 4C–F and Appendix 7. Compared to the modern sample, the Late Pleistocene *M. balthica* shows a much more cemented structure without clear intracrystalline space. The cement is characterized by 50–200 nm sized nanospherulitic shaped crystals (Figures 4D–F). At some locations, these crystals are concentrated in 1-mm-thick elongated zones probably reflecting older, overprinted minerals (Figure 4D). XRMA and XRD results for the Late Pleistocene *M. balthica* are identical to the results for the modern sample (Appendices 8, 9); they too are entirely composed of aragonite. In the Late Pleistocene sample, calcite was absent as well (Table S1). A major difference with the modern sample is that the cemented internal structure of the Late Pleistocene *M. balthica* is characterized by cavities that occur at or near the (polished) surface (Figures 4E–F). The cavities are variable in size but their maximal length does not exceed 20 µm.

SEM photographs of a Late Pleistocene (calcitic) *O. edulis* are presented in Figure 4H. Compared to the modern sample, this shell shows a strongly cemented structure lacking intracrystalline space. Individual crystals are difficult to recognize, although nanospherulitic-shaped crystals appear to be present. XRD results are identical to the modern shell and show a typical calcitic carbonate pattern without evidence for aragonite (Appendix 9).

Holocene Shells

SEM photography of the Holocene shells indicates that the same intracrystalline precipitate as in the Late Pleistocene shell is present in these samples (Appendix 7). The Holocene shells also contain the same cavity-like structures. XRD analysis of the Holocene (aragonitic) samples shows that, similar to the Late Pleistocene samples, all cement is of the same polymorph as the original aragonitic carbonate (Appendix 9; Table S1).

Pliocene Shells

SEM photographs of the two Pliocene aragonitic shells show a pattern of similar intracrystalline cementation (Appendix 7). XRD analysis of the Pliocene (aragonitic) samples shows that, similar to the Late Pleistocene and Holocene samples, all secondary carbonate is of the same polymorph as the original aragonitic carbonate (Appendix 9; Table S1).

$\delta^{13}C/\delta^{18}O$ Isotope Analyses

The $\delta^{13}C/\delta^{18}O$ isotope analysis results for all shell samples are listed in Table S1. $\delta^{18}O$ isotope ratios for the modern samples vary between –0.3 and –1.2‰ (mean –0.4‰). These ratios resemble those of modern-day marine water of the North Sea. The ratio for the modern calcitic sample is slightly higher (0.4‰) but also falls within the range of modern-day North Sea water. $\delta^{18}O$ isotope rations for the Late Pleistocene samples range between –0.8 and –1.6‰ (mean –1.0‰). These ratios are roughly similar to the values for the modern samples. As for the modern samples, the calcitic shell has the highest value.

$\delta^{18}O$ isotope ratios for the Holocene samples range between –2.9 and –3.4‰ (mean –3.2‰). These values are clearly lower than the modern and Late Pleistocene samples. The fact that both $\delta^{13}C$ and $\delta^{18}O$ isotope ratios are also lower for the Holocene samples suggests that there was a higher input of freshwater. The latter is explainable by the paleogeographic setting which, in contrast to modern and Eemian times (Figure 1), indicates the Holocene sample area was located directly within the mouth area of the Rhine-Meuse.

Pyrolysis-Gas Chromatography-Mass Spectrometry

The pyrolysate of the modern *C. edule* was dominated by toluene, phenol, 3- and 4-methylphenol, indole, and 3-methylindole (Figure 5). Together with styrene, these compounds are derived from proteins containing the amino acids tyrosine, phenylalanine, and tryptophan (Tsuge and Matsubaru 1985; Chiavari and Galletti 1992). Small but distinct peaks were identified as diketopiperazines (DKPs) and reflect peptide-derived pyrolysis products of proline and a second amino acid, which included glycine or lysine, proline, and tyrosine (Stankiewicz et al. 1996). Besides a small amount of C_{16} fatty acid, all products point towards "normal" proteins within a modern shell.

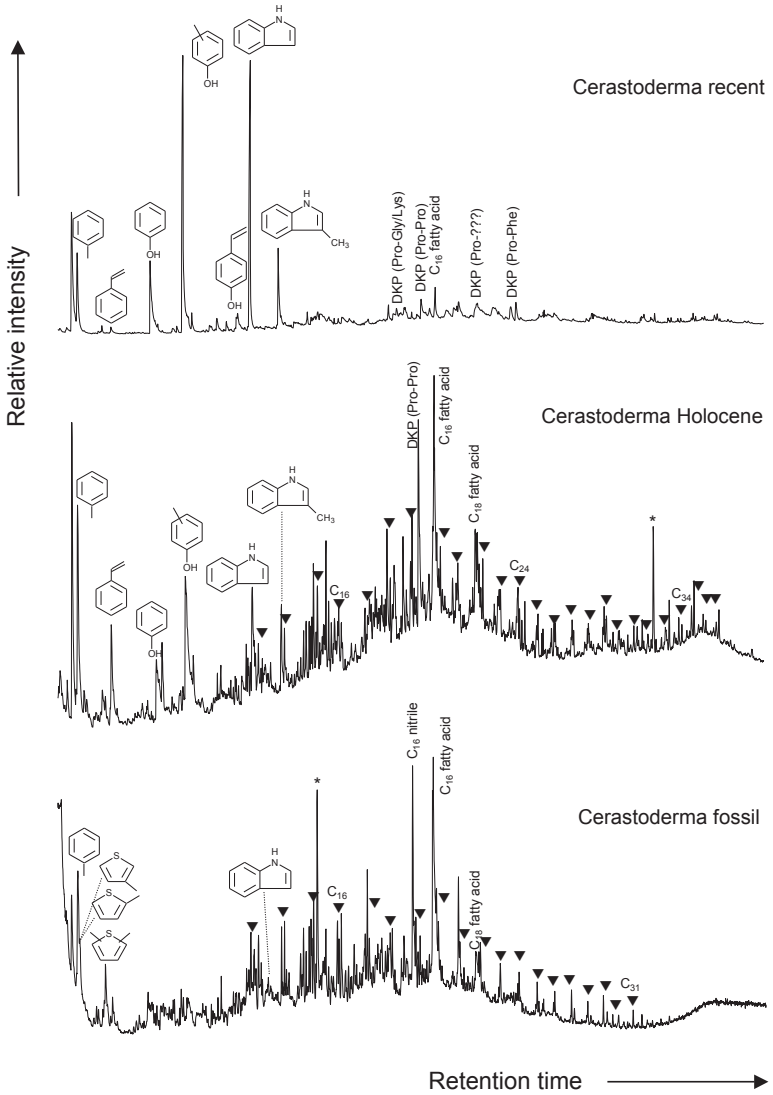

Figure 5 Pyrolysis-gas chromatograms of organic fractions isolated from modern (recent), Holocene, and Late Pleistocene (fossil) *Cerastoderma edule* shells. Legend: filled triangles denote *n*-alkene/*n*-alkane doublet; C_n indicates chain length.

The organic part of the Holocene shell differs significantly from the modern one (Figure 5). The presence of toluene, styrene, phenol, 3- and 4-methylphenol, indole, 3-methylindole, and the DKP of proline-proline in the pyrolysate revealed that proteins were still present in the shell. However, in contrast to the modern one, a homologous series of *n*-alkenes/*n*-alkanes, ranging from C_{13}-C_{37} along with C_{16} and C_{18} fatty acids were highly abundant. Such series of *n*-alkenes/*n*-alkanes are generally attributed to biochemically resistant aliphatic biopolymers and geopolymers. Given their absence from the modern shell, these aliphatic polymers are likely derived from other sources (microorganisms, algae) or formed from (unsaturated) fatty acids through oxidative polymerization (de Leeuw et al. 2006).

The Late Pleistocene *C. edule* shell hardly contains any protein-derived pyrolysis products (toluene, indole), while the *n*-alkenes/*n*-alkanes and fatty acids are still present. In addition, 2- and 3-methylthiophene and several dimethylthiophenes were relatively abundant pyrolysis products (Figure 5). These thiophenes are attributed to sulfurized carbohydrates (e.g. Van Kaam-Peters et al. 1998; Van Dongen et al. 2003) and most likely formed with time under anoxic conditions. From the Pliocene shells, we could not extract enough organic material for analysis.

Overview of Shell Analysis Results

SEM photography shows that the Late Pleistocene shells contain intracrystalline cement. Both the shape of the crystals and cavity-like structures indicate the cement likely formed by bacterial activity. The same features were observed in Holocene shells and Pliocene shells. On the contrary, modern shell shows a much more "open" structure. XRD analysis shows that in the shells the intracrystalline cement is of the same polymorph as the original carbonate. Isotope analysis reveals no major discrepancies in terms of shell type and age. Differences that were observed can be explained by local factors such as the position of the Rhine-Meuse river mouth. All shells except the Pliocene ones show evidence for intracrystalline fatty acids, although in a varying degrading state.

DISCUSSION

Radiocarbon Dating Versus Other Age Constraints

Striking discrepancies are seen between ^{14}C ages and other age constraints in the studied boreholes:

- We observed that the ^{14}C ages of 32–45 ^{14}C kyr BP (indicative of a MIS3 age) were 30 to 100 kyr younger than the quartz and feldspar OSL ages from the sediments in which the shells occur. The latter gave results between 75–130 OSL kyr, which is indicative of MIS5.
- The pollen analysis results show that during deposition of the shell-bearing sediments at the location of core B05G0834, the surrounding vegetation was dominated by full interglacial, deciduous-tree-dominated vegetation. Such a vegetation type is unknown from all studied northwest European MIS3 successions that contain evidence of tundra or steppe with shrubs and grasses (Guiter et al. 2003). The vegetation assemblages of the type encountered in core B05G0834 are only confidently indicative of the Eemian interglacial (~MIS5e; Zagwijn 1996; Cleveringa et al. 2000).
- Furthermore, in core B25E0913 (Appendix 1), we collected a nonfinite, ~45 ^{14}C kyr BP age from the same *V. senescens* shell from which a 118 ± 6 ka age was presented by Van Leeuwen et al. (2000).
- The positions of the shell-bearing estuarine sediments indicate that during the mollusk lifetime, the southern North Sea experienced high sea-level conditions. The uppermost position of *in situ* marine sediments in our cores is –10.5 m asl. A correction of this value by tectonic subsidence

(at least 4 m; calculated using a mean local subsidence rate of 0.1 m/ka; Kooi et al. 1998; Kiden et al. 2002) and a *minimum* age of ~35 ka on the basis of the presented ^{14}C data) and a paleo-water depth estimate of at least several meters, shows that the sea level was positioned close to or above the present mean sea level. We regard this sea-level position as additional strong support for a pre-MIS3 age of the sediments since evidence for an extensive MIS3 marine high stand at levels close to or above the present mean sea level is not observed in eustatic sea-level curves (Waelbroeck et al. 2002; Siddall et al. 2010). Sea levels of the observed magnitude are only confidently indicated for the Eemian interglacial (~MIS5e) and warmer intervals of the Weichselian Early Glacial (MIS5a, MIS5c), all predating ~75 ka. We regard glacio-isostatic crustal movements and/or gravitational effects that could explain the large mismatch between the current elevation of marine sediments and the position of eustatic sea level as highly unlikely. Exceptional suppression-uplift magnitudes and/or gravitational driven sea-level rise would be needed for the MIS3 period that (even) exceed estimates currently known for the Late Pleniglacial (Lambeck 1995; Peltier 2004; Steffen 2006; Vink et al. 2007; Lambeck et al. 2010).

On the basis of the observations presented, we conclude that the ^{14}C outcomes do not represent the true age and reflect minimum ages only. Since we observed no transition towards background ages with increasing dissolution, it can also be concluded that, expect for the Pliocene-age shells, the entire shell structure was contaminated by younger carbon after death and burial of the shells.

Bacterially Mediated Reprecipitation

Wohlfarth et al. (1998) showed that fungi and/or microorganisms can introduce younger (contaminant) ^{14}C in the organic fraction of a sample during storage or preparation. In our case, we disregard these as the source for incorporation of younger carbon because our Pliocene shells, which were stored and pretreated just like all other samples, did give background ages. We neither found evidence for the presence of fungi and/or modern microorganisms in our SEM images.

Post-mortem development of inorganic intracrystalline carbonate cement within a shell structure is regarded a natural cause of introducing younger carbon (Mangerud 1972; Aitken 1990; Webb et al. 2007; Douka et al. 2010). In these studies, recrystallization is essentially described as an inorganic process (only) controlled by the concentrations of both free carbonate and Ca^{2+} ions. Commonly, the secondary precipitant is of the calcite polymorphic state resulting from dissolution of the primary, generally more soluble aragonite. Under specific conditions, with high dissolved Mg^{2+} concentrations (i.e. seawater and/or salt groundwater), (re)precipitation of aragonite over calcite may occur. This (inorganic) recrystallization process is regarded as the prime natural contaminating process for younger C because post-mortem carbonate precipitation can introduce younger ^{14}C from CO_2 that is present in surrounding groundwater and/or air (Mangerud 1972; Appelo and Postma 2005).

Microbial activity is also known to induce or influence the precipitation (and dissolution) of $CaCO_3$ (Castanier et al. 2000; Barabesi et al. 2007; Decho 2010) by modification of a solution (super) saturation state (De Yoreo and Vekilov 2003; Benzerara et al. 2010) and/or providing protected environments (biofilms) where carbonate can mineralize. Several authors describe that the early stage of carbonate precipitation in a biofilm is commonly characterized by the presence of nanoscale spheres (i.e. Dupraz et al. 2004; Benzerara et al. 2010; Decho 2010). Our SEM images of the Late Pleistocene and modern shells clearly show the presence of an intracrystalline precipitate. The nanoscale spheres we observed in our secondary shell carbonate are similar in size and shape as reported in some studies on microorganisms mentioned above, indicating that secondary carbonate precipitation may have occurred in a biofilm environment. Another indication for the presence of a former biofilm environment is formed by the 10–20 μm sized cavities observed in SEM images.

In a biofilm community, gases are produced as a result of bacterial metabolism. The gas can be trapped within the biofilm, forming bubble-shaped and/or lenticular structures or leaving behind "gas-escape" structures (Westall et al. 2001). Characteristic sizes of these pores are similar to those observed in our shells (Ebigbo et al. 2010). The presence of the intracrystalline fatty acids supports the activity of microorganisms in the recrystallization process since bacteria have a wide variety of fatty acids within their membrane (microbial membrane fatty acids or PLFAs) (i.e. Kaneda 1991).

Since the bulk of the shallow groundwater in the Netherlands (<50 m depth) is of Holocene age (Post et al. 2003), Holocene biogenic-induced recrystallization would be an effective contaminator. A total of ~2.5–18% of recrystallized carbonate (assuming a constant recrystallization rate of ~0.2–1.5% per ka for the period 11–0 ka) could explain our ^{14}C dates. If recrystallization took place (somewhere) during MIS3, recrystallization must have affected the entire (100%) shell structure in order to explain the dates. In the latter case, the near identical ^{14}C ages of the intracrystalline noncarbonate fraction and the combined carbonate + noncarbonate fraction ^{14}C age could indicate that the noncarbonate fraction age reflects the remnants of bacteria (or biofilms) that were accountable for the reprecipitation. The bacterial remnants alone (implying a ^{14}C-dead carbonate fraction) cannot explain the dates since their maximal concentration (~0.3% with ~2 $F^{14}C$ ^{14}C) is way too low (Table S1, GrA-53002&53003). The absence of biogenic fatty acids in the (limit) Pliocene samples (Table S1) could indicate that biogenic processes, and hence a potential source for introduction of new ^{14}C, were not active anymore in these samples.

The reason why the biogenic recrystallization process did not change the polymorphic state as well as the isotopic composition of the original MIS5 age shell carbonate is still unknown. One possibility is that bacteria have the capability to (re)precipitate carbonate in a "copy-cat" mode, thereby leaving the chemical and polymorphic signature of the original carbonate intact. A second possibility is that biogenic reprecipitation occurred rapidly after mollusk death when conditions were still (nearly) identical to original mollusk living environment (cf. Douka et al. 2010). Evidence for rapid recrystallization (within several millennia) is shown by the SEM analysis of our Holocene mollusk species. In case of the Late Pleistocene species, this would however mean that recrystallization occurred within MIS5, over 75,000 yr ago, meaning that recrystallization may not be accountable for the nonfinite ^{14}C dates since MIS5-age ^{14}C would all have been decayed. At this stage and with the current data, we cannot solve this puzzling issue.

Although the chemical composition and architecture of other ^{14}C-dated materials is different from marine mollusks, we do suggest that an assessment of possible bacterial imprints in these materials should be part of future analyses. For the southern North Sea, such analyses could help to elucidate the ages of several 30–50 ^{14}C kyr BP bone collagen ^{14}C dates of marine mammals like walrus and beluga as well as of warm-temperate forest animals such as wood elephant (Mol et al. 2006, 2008). The former indicate marine environments during MIS3 when global sea levels where tens of meters lower then the strata from which they derive. The latter represent warm interglacial conditions hitherto known only from MIS5e.

CONCLUSIONS

We present a set of Late Pleistocene marine mollusk ^{14}C (AMS) age estimates of 30–50 ^{14}C kyr BP, whereas a MIS5 age (>75 ka) is indicated by quartz and feldspar OSL dating, biostratigraphy, U-Th dating, and age-depth relationships with sea level. The results indicate that the ^{14}C dates represent minimum ages. The age discrepancy suggests that the shells are contaminated by younger carbon following shell death. The enigmatic ^{14}C dates cannot be "solved" by removing part of the shell by stepwise dissolution. SEM analysis of the Late Pleistocene shells within a context of geologically

younger (recent/modern, Holocene) and older (Pliocene) shells shows the presence of considerable amounts of an intracrystalline secondary carbonate precipitate. The presence of this precipitate is not visible using XRD since it is of the same (aragonitic) polymorph as the original shell carbonate. The combination of nanospherulitic-shaped carbonate crystals, typical cavities, and the presence of fatty acids leads us to conclude that the secondary carbonate, and hence the addition of younger carbon, has a bacterial origin. As we only studied shell material, we recommend an assessment of possible bacterial imprints in other materials like bone collagen as well.

ACKNOWLEDGMENTS

We thank Yusuke Yokoyama, Johannes van der Plicht, and Klaas van der Borg for performing the ^{14}C dating at the laboratories in Tokyo, Groningen, and Utrecht, respectively. Ad van der Spek is thanked for providing the Voorschoten, Stompwijk, and Scheveningen shell samples. Arnold van Dijk and Bernadette Marchand are thanked for the stable isotope analysis. We thank Otto Stiekema for preparing and polishing the SEM samples. Gerard Klaver, Kim Cohen, Jan Peeters, Johan Weijers, Kay Beets, Piet Cleveringa, Alan Decho, and Maarten Lupker are thanked for practical help and/or discussion throughout several stages of this work. All interpretations presented in this paper are those of the authors. The suggestions of three anonymous reviewers greatly helped to improve the structure of the manuscript.

REFERENCES

Aerts-Bijma AT, Meijer HAJ, van der Plicht J. 1997. AMS sample handling in Groningen. *Nuclear Instruments and Methods in Physics Research B* 123(1–4):221–5.

Aerts-Bijma AT, van der Plicht J, Meijer HAJ. 2001. Automatic AMS sample combustion and CO_2 collection. *Radiocarbon* 43(2A):293–8.

Aitken MJ. 1985. *Thermoluminescence Dating*. London: Academic Press.

Aitken MJ. 1990. *Science-Based Dating in Archaeology*. London: Longman.

Alexanderson H, Murray AS. 2012. Luminescence signals from modern sediments in a glaciated bay, NW Svalbard. *Quaternary Geochronology* 10:250–6.

Appelo CAJ, Postma D. 2005. *Geochemistry, Groundwater and Pollution*. Leiden: A. A. Balkema.

Ballarini M, Wintle AG, Wallinga J. 2006. Spatial variation of dose rate from beta sources as measured using single grains. *Ancient TL* 24(1):1–8.

Ballarini M, Wallinga J, Wintle AG, Bos AJJ. 2007. A modified SAR protocol for optical dating of individual grains from young quartz samples. *Radiation Measurements* 42(3):360–9.

Barabesi C, Galizzi A, Mastromei G, Rossi M, Tamburini E, Perito B. 2007. *Bacillus subtilus* gene cluster involved in calcium carbonate biomineralization. *Journal of Bacteriology* 189(1):228–35.

Benzerara K, Menguy N, López-García P, Yoon TH, Kazmierczak J, Tyliszczak T, Brown Jr GE. 2006. Nanoscale detection of organic signatures in carbonate microbialites. *Proceedings of the National Academy of Sciences of the USA* 103(25):9440–5.

Bish DL, Post JE. 1993. Quantitative mineralogical analysis using the Rietveld full-pattern fitting method. *American Mineralogist* 78(9–10):932–40.

Bøtter-Jensen L, Andersen CE, Duller GAT, Murray AS. 2003. Developments in radiation, stimulation and observation facilities in luminescence measurements. *Radiation Measurements* 37(4–5):535–41.

Braucher R, Bourlès D, Merchel S, Vidal Romani J, Fernadez-Mosquera D, Marti K, Léanni L, Chauvet F, Arnold M, Aumaître G, Keddadouche K. 2013. Determination of muon attenuation lengths in depth profiles from in situ produced cosmogenic nuclides. *Nuclear Instruments and Methods in Physics Research B* 294:484–90.

Bunnik FPM. 2008. *Pollenanalyses van boring Lutjelollum (Fr.) (B05G0834)*. TNO-report 2008-U-R0631/A. Utrecht: TNO. In Dutch.

Busschers FS, Weerts HJT, Wallinga J, Cleveringa P, Kasse C, de Wolf H, Cohen KM. 2005. Sedimentary architecture and optical dating of Middle and Late Pleistocene Rhine-Meuse deposits – fluvial response to climate change, sea-level fluctuation and glaciation. *Netherlands Journal of Geosciences* 84(1):25–41.

Busschers FS, Kasse C, van Balen RT, Vandenberghe J, Cohen KM, Weerts HJT, Wallinga J, Johns C, Cleveringa P, Bunnik FPM. 2007. Late Pleistocene evolution of the Rhine-Meuse system in the Southern North Sea basin: imprints of climate change, sea-level oscillation and glacio-isostacy. *Quaternary Science Reviews* 26(25–28):3216–48.

Busschers FS, Van Balen RT, Cohen KM, Kasse C, Weerts HJT, Wallinga J, Bunnik FPM. 2008. Response of the Rhine-Meuse fluvial system to Saalian ice-sheet dynamics. *Boreas* 37(3):377–98.

Buylaert J-P, Murray AS, Thomsen KJ, Jain M. 2009. Testing the potential of an elevated temperature IRSL signal from K-feldspar. *Radiation Measurements* 44(5–6):560–5.

Buylaert J-P, Jain M, Murray AS, Thomsen KJ, Thiel C, Sohbati R. 2012. A robust feldspar luminescence dating method for Middle and Late Pleistocene sediments. *Boreas* 41(3):435–51.

Castanier S, Le Méteyer-Levrel G, Martire L. 2000. Bacterial roles in the precipitation of carbonate minerals. In: Riding RE, Awramik SM, editors. *Microbial Sediments*. Heidelberg: Springer. p 32–9.

Chiavari G, Galletti GC. 1992. Pyrolysis-gas chromatography/mass spectrometry of amino acids. *Journal of Analytical and Applied Pyrolysis* 24(2):123–37.

Cleveringa P, Meijer T, Van Leeuwen RJW, De Wolf H, Pouwer R, Lissenberg T, Burger AW. 2000. The Eemian stratotype locality at Amersfoort in the central Netherlands: a re-evaluation of old and new data. *Geologie en Mijnbouw* 79:197–216.

Cunningham AC, Wallinga J. 2010. Selection of integration time intervals for quartz OSL decay curves. *Quaternary Geochronology* 5(6):657–66.

Dandurand JL, Gout R, Schott J. 1982. Experiments on phase transformations and chemical reactions of mechanically activated minerals by grinding: petrogenetic implications. *Tectonophysics* 83(3–4):365–86.

Decho AW. 2010. Overview of biopolymer-induced mineralization: What goes on in biofilms? *Ecological Engineering* 36(2):137–44.

De Gans W, Beets DJ, Centineo MC. 2000. Late Saalian and Eemian deposits in the Amsterdam glacial basin. *Geologie en Mijnbouw* 79:147–60.

de Leeuw JW, Versteegh GJM, Van Bergen PF. 2006. Biomacromolecules of algae and plants and their fossil analogues. *Plants and Climate Change* 182:209–33.

De Yoreo JJ, Vekilov PG. 2003. Principles of crystal nucleation and growth. *Reviews in Mineralogy and Geochemistry* 54(1):57–93.

Douka K, Hedges REM, Higham TFG. 2010. Improved AMS ^{14}C dating of shell carbonates using high-precision X-ray diffraction and novel density separation protocol (CarDS). *Radiocarbon* 52(2–3):735–51.

Dupraz C, Visscher PT, Baumgartner LK, Reid RP. 2004. Microbe-mineral interactions: early carbonate precipitation in a hypersaline lake (Eleuthera Island, Bahamas). *Sedimentology* 51(4):745–65.

Ebigbo A, Helmig R, Cunningham AB, Class H, Gerlach R. 2010. Modelling biofilm growth in the presence of carbon dioxide and water flow in the subsurface. *Advances in Water Resources* 33(7):762–81.

Gammage RB, Glasson DR. 1976. The effect of grinding on the polymorphs of calcium carbonate. *Journal of Colloid and Interface Science* 55(2):396–401.

Goslar T, Pazdur MF. 1985. Contamination studies on mollusk shell samples. *Radiocarbon* 27(1):33–42.

Gosse JC, Philips FM. 2001. Terrestrial in situ cosmogenic nuclides: theory and application. *Quaternary Science Reviews* 20(14):1475–560.

Guiter F, Andrieu-Ponel V, De Beaulieu JL, Ceddadi R, Calvez M, Ponel P, Reille M, Keller T, Goeury C. 2003. The last climatic cycles in Western Europe: a comparison between long continuous lacustrine sequences from France and other terrestrial records. *Quaternary International* 111(1):59–74.

Hijma MP, Cohen KM, Hoffmann G, Van der Spek AJF, Stouthamer E. 2009. From river valley to estuary: the evolution of the Rhine mouth in the early to middle Holocene (western Netherlands, Rhine-Meuse delta). *Netherlands Journal of Geosciences* 88(1):13–53.

Huntley DJ, Baril MR. 1997. The K content of the K-feldspars being measured in optical dating or in thermoluminescence dating. *Ancient TL* 15(1):11–3.

Huntley DJ, Hancock RGV. 2001. The Rb contents of the K-feldspar grains being measured in optical dating. *Ancient TL* 19:43–6.

Huntley DJ, Lamothe M. 2001. Ubiquity of anomalous fading in K-feldspars and the measurement and correction for it in optical dating. *Canadian Journal of Earth Science* 38(7):1093–106.

Kaneda T. 1991. Iso- and anteiso-fatty acids in bacteria: biosynthesis, function, and taxonomic significance. *Microbiology and Molecular Biology Reviews* 55(2):288–302.

Kars RH, Busschers FS, Wallinga J. 2012. Validating post IR-IRSL dating on K-feldspars through comparison with quartz OSL ages. *Quaternary Geochronology* 12:74–86.

Kars RH, Wallinga J. 2009. IRSL dating of K-feldspars: modelling natural dose response curves to deal with anomalous fading and trap competition. *Radiation Measurements* 44(5–6):594–9.

Kars RH, Wallinga J, Cohen KM. 2008. A new approach towards anomalous fading correction for feldspar IRSL dating – tests on samples in field saturation. *Radiation Measurements* 43(2–6):786–90.

Kiden P, Denys L, Johnston P. 2002. Late Quaternary sea-level change and isostatic and tectonic land movements along the Belgian-Dutch North Sea coast: geological data and model results. *Journal of Quaternary Science* 17(5–6):535–46.

Kooi H, Johnston P, Lambeck K, Smither C, Molendijk R. 1998. Geological causes of recent (~100 yr) vertical land movement in the Netherlands. *Tectonophysics* 299(4):297–316.

Lambeck K. 1995. Late Devensian and Holocene shorelines of the British Isles and North Sea from models of glacio-hydro-isostatic rebound. *Journal of the Geological Society of London* 152(3):437–48.

Lambeck K, Purcell A, Zhao J, Svensson N-O. 2010. The Scandinavian Ice Sheet: from MIS 4 to the end of the Last Glacial Maximum. *Boreas* 39(2):410–35.

Lamothe M, Auclair M, Hamzaoui C, Huot S. 2003. Towards a prediction of long-term anomalous fading of feldspar IRSL. *Radiation Measurements* 37(4–5):493–8.

Magnani G, Bartolomei P, Cavulli F, Esposito M, Marino EC, Neri M, Rizzo A, Scaruffi S, Tosi M. 2007. U-series and radiocarbon dates on mollusk shells from the uppermost layer of the archaeological site of KHB-1, Ra's al Khabbah, Oman. *Journal of Archaeological Science* 34(5):749–55.

Mangerud J. 1972. Radiocarbon dating of marine mollusks, including discussion of apparent age of recent mollusks from Norway. *Boreas* 1(2):143–72.

Matsuzaki H, Nakano C, Yamashita H, Maejima Y, Miyairi Y, Wakasa S, Horiuchi K. 2004. Current status and future direction of MALT, The University of Tokyo. *Nuclear Instruments and Methods in Physics Research B* 223–224:92–9.

Meijer T. 2008. Molluskenonderzoek van boring Lutjelollum-5G834. Palaeomal, WMC Kwartair Consultants, Rapport M24, 1-6, 1 addendum. In Dutch.

Meijer T, Cleveringa P. 2009. Aminostratigraphy of Middle and Late Pleistocene deposits in The Netherlands and the southern part of the North Sea Basin. *Global and Planetary Change* 68(4):326–45.

Meijer T, Preece RC. 1995. Malacological evidence relating to the insularity of the British Isles during the Quaternary. In: Preece RC, editor. *Island Britain: A Quaternary Perspective*. London: Geological Society Special Publication 96. p 89–110.

Mejdahl V. 1987. Internal radioactivity in quartz and feldspar grains. *Ancient TL* 5(2):10–7.

Moerdijk PW, Janssen AW, Wesselingh FP, Peeters GA, Pouwer R, van Nieulande FAD, Janse AC, van der Slik L, Meijer T, Rijken R, Cadee GC, Hoeksema D, Doeksen G, Bastemeijer A, Strack H, Vervoenen M, ter Poorten JJ. 2010. *De fossiele schelpen van de Nederlandse kust*. Leiden: NCB Naturalis.

Mol D, Post K, Reumer JWF, van der Plicht H, de Vos J, van Geel B, van Reenene G, Pals JP, Glimmerveen J. 2006. The Eurogeul - first report of the palaeontological, palynological and archaeological investigations of this part of the North Sea. *Quaternary International* 142–143:178–85.

Mol D, de Vos J, Bakker R, van Geel B, Glimmerveen J, van der Plicht H, Post K. 2008. *Kleine encyclopedie van het leven in het Pleistoceen: mammoeten, neushoorns en andere dieren van de Noordzeebodem*. Diemen: Veen Magazines.

Morthekai P, Jain M, Murray AS, Thomsen KJ, Bøtter-Jensen L. 2008. Fading characteristics of martian analogue materials and the applicability of a correction procedure. *Radiation Measurements* 43(2–6):672–8.

Murray A, Buylaert J-P, Henriksen M, Svendsen J-I, Mangerud J. 2008. Testing the reliability of quartz OSL ages beyond the Eemian. *Radiation Measurements* 43(2–6):776–80.

Murray AS, Wintle AG. 2000. Luminescence dating of quartz using an improved single-aliquot regenerative-dose protocol. *Radiation Measurements* 32(1):57–73.

Murray AS, Wintle AG. 2003. The single aliquot regenerative dose protocol: potential for improvements in reliability. *Radiation Measurements* 37(4–5):377–81.

Murray AS, Buylaert J-P, Thomsen KJ, Jain M. 2009. The effect of preheating on the IRSL signal from feldspar. *Radiation Measurements* 44(5–6):554–9.

Nadeau M-J, Grootes MP, Voelker A, Bruhn F, Duhr A, Oriwall A. 2001. Carbonate ^{14}C background: Does it have multiple personalities? *Radiocarbon* 43(2A):169–76.

Peltier WR. 2004. Global glacial isostasy and the surface of the ice-age Earth: the ICE-5G (VM2) model and GRACE. *Annual Review of Earth and Planetary Sciences* 32:111–49.

Pesenti H, Leoni M, Scardi P. 2008. XRD line profile analysis of calcite powders produced by high energy milling. *Zeitschrift fur Kristallographie Supplement* 27:143–50.

Post VEA, van der Plicht H, Meijer HAJ. 2003. The origin of brackish and saline groundwater in the coastal area of the Netherlands. *Netherlands Journal of Geosciences* 82(2):133–47.

Prescott JR, Hutton JT. 1994. Cosmic ray contributions to dose rates for luminescence and ESR dating: large depths and long-term time variations. *Radiation Measurements* 23(2–3):497–500.

Price GJ, Webb GE, Zhao J. 2011. Dating megafaunal extinction on the Pleistocene Darling Downs, eastern Australia: the promise and pitfalls of dating as a test of extinction hypotheses. *Quaternary Science Reviews* 30(7–8):899–914.

Reimann T, Tsukamoto S. 2012. Dating the recent past (<500 years) by post-IR IRSL feldspar – examples from the North Sea and Baltic Sea coast. *Quaternary Geochronology* 10:180–7.

Rietveld HM. 1969. A profile refinement method for nuclear and magnetic structures. *Journal of Applied Crystallography* 2:65–71.

Rozanski K, Stichler W, Gonfiantini R, Scott EM, Beukens RP, Kromer B, van der Plicht J. 1992. The IAEA ^{14}C Intercomparison Exercise 1990. *Radiocarbon* 34(3):506–19.

Siddall M, Kaplan MR, Schaefer JM, Putnam A, Kelly MA, Goehring B. 2010. Changing influence of Antarctic and Greenland temperature records on sea level over the last glacial cycle. *Quaternary Science Reviews* 29(3–4):410–23.

Stankiewicz BA, van Bergen PF, Duncan IJ, Carter JF, Briggs DEG, Evershed RP. 1996. Recognition of chitin and proteins in invertebrate cuticles using analytical pyrolysis/gas chromatography/mass spectrometry. *Rapid Communications in Mass Spectrometry* 10(14):1747–57.

Steffen H. 2006. Determination of a consistent viscosity distribution in the Earth's mantle beneath Northern and Central Europe [PhD dissertation]. Berlin: Institut für Geologische Wissenschaften der Freie Universität Berlin.

Thiel C, Buylaert J-P, Murray A, Terhorst B, Hofer I, Tsukamoto S, Frechen M. 2011. Luminescence dating of the Stratzing loess profile (Austria) – testing the potential of an elevated temperature post-IR IRSL protocol. *Quaternary International* 234(1):23–31.

Thomsen KJ, Murray AS, Jain M, Bøtter-Jensen L. 2008. Laboratory fading rates of various luminescence signals from feldspar-rich sediment extracts. *Radiation Measurements* 43(9–10):1474–86.

Törnqvist TE, Wallinga J, Murray AS, De Wolf H, Cleveringa P, De Gans W. 2000. Response of the Rhine-Meuse system (west-central Netherlands) to the last Quaternary glacio-eustatic cycles: a first assessment. *Global and Planetary Change* 27(1–4):89–111.

Törnqvist TE, Wallinga J, Busschers FS. 2003. Timing of the last sequence boundary in a fluvial setting near the highstand shoreline – insights from optical dating. *Geology* 31(3):279–82.

Tsuge S, Matsubara H. 1985. High-resolution pyrolysis-gas chromatography of proteins and related materials. *Journal of Analytical and Applied Pyrolysis* 8:49–64.

Van der Borg K, Alderliesten C, de Jong AFM, van den Brink A, de Haas AP, Kersemaekers HJH, Raaymakers JEMJ. 1997. Precision and mass fractionation in ^{14}C with AMS. *Nuclear Instruments and Methods in Physics Research B* 123(1–4):97–101.

van der Plicht J, Wijma S, Aerts AT, Pertuisot MH, Meijer HAJ. 2000. Status report: the Groningen AMS facility. *Nuclear Instruments and Methods in Physics Research B* 172(1–4):58–65.

van der Plicht J. 2012. Borderline radiocarbon. *Netherlands Journal of Geosciences* 91(1–2):257–61.

Van Dongen BE, Schouten S, Baas M, Geenevasen AJ, Sinninghe Damsté JS. 2003. An experimental study of the low-temperature sulfurization of carbohydrates. *Organic Geochemistry* 34(8):1129–44.

Van Kaam-Peters HME, Schouten S, Köster J, Sinninghe Damsté JS. 1998. Controls on the molecular and carbon isotopic composition of organic matter deposited in a Kimmeridgian euxinic shelf sea: evidence for preservation of carbohydrates through sulfurisation. *Geochimica et Cosmochimica Acta* 62(19–20):3259–83.

Van Leeuwen RJW, Beets DJ, Bosch JHA, Burger AW, Cleveringa P, Van Harten D, Herngreen GFW, Kruk RW, Langereis CG, Meijer T, Pouwer R, De Wolf H. 2000. Stratigraphy and integrated facies analysis of the Saalian and Eemian sediments in the Amsterdam-Terminal borehole, the Netherlands. *Geologie en Mijnbouw* 79:161–96.

Van Santvoort PJM, De Lange GJ, Thomson J, Colley S, Meysman FJR, Slomp CP. 2002. Oxidation and origin of organic matter in surficial Eastern Mediterranean hemipelagic sediments. *Aquatic Geochemistry* 8(3):153–75.

Vink A, Steffen H, Reinhardt L, Kaufmann G. 2007. Holocene relative sea-level change, isostatic subsidence and the radial viscosity structure of the mantle of northwest Europe (Belgium, the Netherlands, Germany, southern North Sea). *Quaternary Science Reviews* 26(25–28):3249–75.

Waelbroeck C, Labeyrie L, Michel E, Duplessy JC, McManus JF, Lambeck K, Balbon E, Labracherie M. 2002. Sea-level and deep water temperature changes derived from benthic foraminifera isotopic records. *Quaternary Science Reviews* 21(1–3):295–305.

Wallinga J. 2002. Optically stimulated luminescence dating of fluvial deposits: a review. *Boreas* 31(4):303–22.

Wallinga J, Murray AS, Bøtter-Jensen L. 2002. Measurement of the dose in quartz in the presence of feldspar contamination. *Radiation Protection Dosimetry* 101(1–4):367–70.

Wallinga J, Tornqvist TE, Busschers FS, Weerts HJT. 2004. Allogenic forcing of the late Quaternary Rhine-Meuse fluvial record: the interplay of sea-level change, climate change and crustal movements. *Basin Research* 16(4):535–47.

Webb GE, Price GJ, Nothdurft LD, Deer L, Rintoul L. 2007. Cryptic meteoric diagenesis in freshwater bivalves: implications for radiocarbon dating. *Geology* 35(9):803–6.

Westall F, de Wit MJ, Dann J, Van der Gaast S, de Ronde CEJ, Geneke D. 2001. Early Archean fossil bacteria and biofilms in hydrothermally influenced, shallow water sediments, Barberton Greenstone Belt, South Africa. *Precambrian Research* 106(1–2):93–116.

Westerhoff WE, Wong TE, Geluk MC. 2003. De opbouw van de ondergrond. In: De Mulder EFJ, Geluk MC, Ritsema I, Westerhoff WE, Wong TE, editors. *De ondergrond van Nederland*. Nederlands Instituut voor Toegepaste Geowetenschappen TNO, Geologie van Nederland 7. p 247–352.

Wintle AG. 1973. Anomalous fading of thermoluminescence in mineral samples. *Nature* 245(5421):143–4.

Wintle AG, Murray AS. 2006. A review of quartz optically stimulated luminescence characteristics and their relevance in single-aliquot regeneration dating protocols. *Radiation Measurements* 41(4):369–91.

Wohlfarth B, Skog G, Possnert G, Holmquist B. 1998. Pitfalls in the AMS radiocarbon-dating of terrestrial macrofossils. *Journal of Quaternary Science* 13(2):137–45.

Yokoyama Y, Miyairi Y, Matsuzaki H, Tsunomori F. 2007. Relation between acid dissolution time in the vacuum test tube and time required for graphitization for AMS target preparation. *Nuclear Instruments and Methods in Physics Research B* 259(1):330–4.

Zagwijn WH. 1961. Vegetation, climate and radiocarbon datings in the Late Pleistocene of the Netherlands, Part I: Eemian and Early Weichselian. *Mededelingen Geologische Stichting N.S* 14:15–45.

Zagwijn WH. 1996. An analysis of Eemian climate in western and central Europe. *Quaternary Science Reviews* 15(5–6):451–69.